

WestminsterResearch

<http://www.westminster.ac.uk/westminsterresearch>

**Detailed phenotypic and genotypic characterization of bietti
crystalline dystrophy**

**Halford, S., Liew, G., Mackay, D.S., Sergouniotis, P.I., Holt, R.,
Broadgate, S., Volpi, E., Ocaka, L., Robson, A.G., Holder, G.E.,
Moore, A.T., Michaelides, M. and Webster, A.R.**

NOTICE: this is the authors' version of a work that was accepted for publication in Ophthalmology. Changes resulting from the publishing process, such as peer review, editing, corrections, structural formatting, and other quality control mechanisms may not be reflected in this document. Changes may have been made to this work since it was submitted for publication. A definitive version was subsequently published in Ophthalmology, 121 (6), pp. 1174-1184, 2014.

The final definitive version in Ophthalmology is available online at:

<https://dx.doi.org/10.1016/j.ophtha.2013.11.042>

© 2014. This manuscript version is made available under the CC-BY-NC-ND 4.0 license

<http://creativecommons.org/licenses/by-nc-nd/4.0/>

The WestminsterResearch online digital archive at the University of Westminster aims to make the research output of the University available to a wider audience. Copyright and Moral Rights remain with the authors and/or copyright owners.

Whilst further distribution of specific materials from within this archive is forbidden, you may freely distribute the URL of WestminsterResearch: (<http://westminsterresearch.wmin.ac.uk/>).

In case of abuse or copyright appearing without permission e-mail repository@westminster.ac.uk

1
2
3
4
5
6
7
8
9
10
11
12
13
14
15
16
17
18
19
20
21
22
23
24
25
26
27

Detailed Phenotypic and Genotypic Characterization of Bietti Crystalline Dystrophy

Short title: Phenotypic and Genetic Findings in Bietti Dystrophy

Stephanie Halford, PhD,^{*1} Gerald Liew, PhD,^{*2,3} Donna S. Mackay, PhD,³ Panagiotis I. Sergouniotis, PhD,^{3,4}
Richard Holt, DPhil,¹ Suzanne Broadgate, PhD,¹ Emanuela V. Volpi, PhD,^{5†} Louise Ocaka, PhD,⁶ Anthony G.
Robson, PhD,^{3,4} Graham E. Holder, PhD,^{3,4} Anthony T. Moore, MD,^{3,4} Michel Michaelides, MD,^{3,4} and
Andrew R. Webster, MD.^{3,4}

¹ Nuffield Laboratory of Ophthalmology, Nuffield Department of Clinical Neuroscience, University of Oxford, Headley Way. Oxford. OX3 9DU, UK

² Centre for Vision Research, Westmead Millennium Institute, University of Sydney, Sydney. Australia

³ Moorfields Eye Hospital, London. EC1V 2PD, UK

⁴ University College London, Institute of Ophthalmology, Bath Street, London EC1V 9EL, UK;

⁵ Molecular Cytogenetics and Microscopy Core, Wellcome Trust Centre for Human Genetics, University of Oxford, Roosevelt Drive, Oxford, OX3 7BN, UK.

⁶ Institute of Child Health, Guilford Street. London. WC1N 1EH, UK.

[†]Current address: Department of Biomedical Sciences, Faculty of Science and Technology, University of Westminster, 115 New Cavendish Street, London, W1W 6UW, UK

*Both Stephanie Halford, PhD, and Gerald Liew, PhD, have contributed equally to this work

Financial Disclosure(s):

The authors have no proprietary or commercial interest in any materials discussed in this article.

28 **Sources of Funding:**

29 The work was supported by grants from the National Institute for Health Research Biomedical Research
30 Centre at Moorfields Eye Hospital National Health Service Foundation Trust and UCL Institute of
31 Ophthalmology, Fight For Sight (UK) and FFS Mercer Fund, Moorfields Eye Hospital Special Trustees,
32 Macular Disease Society, the Foundation Fighting Blindness (USA), and Retinitis Pigmentosa Fighting
33 Blindness. EmanuelaVolpi was supported by the Wellcome Trust [Wellcome Trust Core Award Grant
34 number 090532/Z/09/Z], Michel Michaelides is supported by an FFB Career Development Award. There is
35 no conflict of interest. The sponsors or funding organizations had no role in the design or conduct of this
36 research.

37

38 **Corresponding authors**

- 39 1. Stephanie Halford, Nuffield Laboratory of Ophthalmology, Nuffield Department of Clinical
40 Neuroscience, University of Oxford, Level 6 John Radcliffe Hospital, Headley Way. Oxford, OX3 9DU,
41 UK. Tel: +44 1865 234704, E-mail: stephanie.halford@eye.ox.ac.uk
- 42 2. Andrew Webster, University College London, Institute of Ophthalmology, Bath Street, London EC1V
43 9EL, UK. Tel: +44 20 7566 2278, E-mail: andrew.webster@ucl.ac.uk

44

45 Word count: 5340

46

47 **Abstract**

48 Objective: To provide a detailed phenotype/genotype characterization of Bietti Crystalline Dystrophy (BCD).

49 Design: Observational case series.

50 Participants: Twenty patients from 17 families recruited from a multi-ethnic British population.

51 Methods: Patients underwent color fundus photography, near infra-red (NIR) imaging, fundus
52 autofluorescence (AF) imaging, spectral domain-optical coherence tomography (SD-OCT) and
53 electroretinogram (ERG) assessment. The gene *CYP4V2* was sequenced.

54 Main Outcome Measures: Clinical, imaging, electrophysiological and molecular genetics findings.

55 Results: Patients ranged in age from 19 to 72 years (median 40), with visual acuity of 6/5 to perception of
56 light (median 6/12). There was wide intra- and inter-familial variability in clinical severity. Fundus AF
57 imaging showed well defined areas of retinal pigment epithelium (RPE) loss which corresponded on SD-OCT
58 to well demarcated areas of outer retinal atrophy. Retinal crystals were not evident on fundus AF imaging,
59 and were best visualized with NIR imaging. SD-OCT showed them to be principally located on or in the
60 RPE/Bruch's membrane complex. Disappearance of the crystals, revealed by serial recording, was
61 associated with severe disruption and thinning of the RPE/Bruch's membrane complex. Cases with
62 extensive RPE degeneration (N=5) had ERGs consistent with generalized rod and cone dysfunction, but
63 those with more focal RPE atrophy either showed amplitude reduction without delay (N=3), consistent with
64 restricted loss of function, or were normal (N=2). Likely disease-causing variants were identified in 34
65 chromosomes from 17 families. Seven were novel including p.Met66Arg, found in all 11 patients from 8
66 families of South Asian descent. This mutation appears to be associated with earlier onset (median age 30)
67 compared to other substitutions (median age 41). Deletions of exon 7 were associated with more severe
68 disease.

69 Conclusions: The phenotype is highly variable. Several novel variants are reported, including a highly
70 prevalent substitution in patients of South Asian descent associated with earlier onset disease. AF showed
71 sharply demarcated areas of RPE loss which coincided with abrupt edges of outer retinal atrophy on SD-
72 OCT; crystals were generally situated on or in the RPE/Bruch's complex but could disappear over time with
73 associated RPE disruption. These results support a role for the RPE in disease pathogenesis.

74

75 **Introduction**

76 Bietti crystalline corneoretinal dystrophy (BCD, Online Mendelian Inheritance in Man (OMIM) 210370) is a
77 rare autosomal recessive disease that is characterized by yellow-white crystalline retinal deposits,
78 progressive atrophy of the retinal pigment epithelium (RPE) and loss of choriocapillaris. In some patients,
79 but not all, this is accompanied by crystalline deposits at the corneal limbus.¹ BCD typically presents
80 between the second and fourth decade with progressive night blindness, reduced vision and visual field
81 constriction, often with legal blindness in the fifth or sixth decades of life.¹ In 2000 Jiao *et al* mapped BCD to
82 chromosome 4q35.1² and subsequently Li and colleagues identified disease-causing variants in *CYP4V2*, a
83 novel member of the cytochrome P450 gene family (family 4, subfamily V, polypeptide 2).³

84 The majority of phenotypic data are derived from a small number of case reports and case series, with the
85 largest series to date describing 21 patients.⁴⁻⁹ The main characteristics and natural history of the disease
86 are reasonably well characterized, but there remain areas of uncertainty, including the precise intraretinal
87 location of the crystals and primary pathology, the degree of variability and its association, if any, with the
88 underlying mutations, the pattern of cell loss and its retinal distribution. There is limited information on the
89 time course of crystal formation within the retina and few studies have described the retinal characteristics
90 using newer imaging modalities such as near infra-red (NIR) imaging and spectral domain optical coherence
91 tomography (SD-OCT).

92 This report describes the detailed clinical features and molecular pathology in a cohort of 20 patients from
93 17 families affected by BCD from a British multi-ethnic population, and examines the relationship between
94 disease-causing variants and disease severity.

95

96 **Methods**

97 Twenty patients with a clinical diagnosis of BCD were ascertained from Moorfields Eye Hospital, London,
98 United Kingdom over a 13-year period from 1999 to 2012. Patients were recruited from one of three
99 ophthalmologists' clinics (ARW, ATM, MM) and included in the study only if all clinical data were consistent
100 with the diagnosis. This was later confirmed with *CYP4V2* sequencing. Patients provided informed consent
101 as part of a research project approved by the local research ethics committee, and all investigations were

102 conducted in accordance with the principles of the Declaration of Helsinki. One patient (case 19) has been
103 described previously.⁶

104 *Clinical studies:*

105 All patients had their clinical history documented and underwent eye examinations which included best-
106 corrected visual acuity, slit lamp biomicroscopy, dilated fundus examination and digital fundus photography
107 (TRC-501A; Topcon, Tokyo, Japan). The severity of fundus appearance was graded according to the scale
108 proposed by Yuzawa et al.¹⁰ and simplified by Weleber and Wilson¹¹ which describes 3 stages of increasing
109 severity – stage 1: RPE atrophy only; stage 2: RPE and choroidal atrophy localized to the macular region;
110 stage 3: RPE and choroidal atrophy extending beyond the macula. Severity grading was performed by one
111 investigator (GL) and independently checked by another (AGR). Disagreements were adjudicated through
112 discussion and the consensus grading was used. Imaging studies were addressed in a similar fashion.

113 *Imaging:*

114 The Spectralis HRA + OCT with viewing module version 5.1.2.0 (Heidelberg Engineering, Heidelberg,
115 Germany) was used to acquire autofluorescence (AF) images over 30x30° and 55x55° fields as well as SD-
116 OCT images. Fundus autofluorescence imaging (FAF) was available in 17 patients; SD-OCT in fifteen
117 patients; 11 patients had longitudinal data available. The SD-OCT protocol included a dense horizontal
118 linear scan centered on the fovea and the HEYEX software interface (version 1.6.2.0; Heidelberg
119 Engineering) was used to correlate position markers on NIR and SD-OCT scanning to localize lesions. The
120 same program also allows registration of blood vessels from the NIR images to facilitate longitudinal
121 analysis of crystal evolution. The location of crystals was correlated across color photographs, NIR, AF and
122 SD-OCT imaging using side-by-side comparisons, and where available, HEYEX position markers.
123 Observations had to be replicated in at least two patients before they were accepted as valid and described
124 in this study.

125 *Electrophysiology:*

126 Eleven patients underwent electrophysiological assessment using full field electroretinography (ERG) and
127 pattern ERG. All protocols incorporated the recommendations of the International Society for Clinical
128 Electrophysiology of Vision (ISCEV) standards.¹²⁻¹⁴

129 *CYP4V2 mutation screening*

130 Blood samples were collected and DNA was extracted using the Puregene blood extraction kit (Invitrogen,
131 Paisley, UK) following manufacturer's instructions. Each of the 11 exons of CYP4V2 was amplified from
132 patient genomic DNA using primers located in the flanking intron and untranslated regions. The primers
133 and conditions were as described previously³ and allowed each exon, including splice junctions to be
134 amplified.

135 The products were purified using Qiagen polymerase chain reaction (PCR) purification columns (Qiagen, UK)
136 and sequenced using the fluorescently-labeled dideoxy-terminator method on an ABI 3100 Automated DNA
137 Sequencer (Applied Biosystems, UK). Electropherograms were analyzed for sequence changes using
138 DNASTar computational software (DNASTar, Inc., USA). Sequencing data obtained from PCR products were
139 analyzed using SeqMan, a program designed to detect potential alterations in the sequence. Any sequence
140 changes identified were checked visually. When family samples were available the segregation of
141 potentially disease-causing variants was investigated. Missense mutations were analyzed using three
142 software prediction programs:

143 SIFT (Sorting Intolerant from Tolerance) (J. Craig Venter Institute; Available at: <http://sift.jcvi.org/>. Accessed
144 August 1, 2013.), PolyPhen2 (Available at: <http://genetics.bwh.harvard.edu/pph/index.html>. Accessed
145 August 1, 2013) and pMUT (University of Barcelona Molecular Recognition & Bioinformatics Group;
146 Available at: <http://mmb.pcb.ub.es/PMut/>. August 1, 2013) splice mutations were analysed using
147 NetGene2 (Technical University of Denmark Center for Biological Sequence Analysis; Available at:
148 <http://www.cbs.dtu.dk/services/NetGene2/> Accessed October 15, 2013).

149 *Fluorescence in situ hybridization (FISH)*

150 Chromosome slides for FISH analysis were obtained from peripheral blood lymphocyte cultures following
151 standard cytogenetic procedures. Prior to the hybridization the slides were denatured in 70% formamide at
152 70°C for 2 minutes, quenched in 2xSSC at 4°C and then dehydrated in an ethanol series. The FITC-labeled
153 BAC probe 173M11 (Empire Genomics) was co-hybridized to the slides with a TRITC-labeled chromosome 4
154 specific "paint" (Cambio). Hybridization and post-hybridization washes were carried out following the
155 manufacturers' instructions. The slides were mounted with Vectashield (Vector Laboratories) containing 4',

156 6-diamidino-2-phenylindole (DAPI) for chromosome counterstaining. Image capture and analysis were
157 carried out on a CytoVysion system (Genetix) consisting of an Olympus BX-51 epifluorescence microscope
158 coupled to a JAI CVM4+ CCD camera. At least 30 informative metaphases per sample were captured and
159 analyzed.

160 *Comparative genomic hybridization (CGH)*

161 Array CGH was used to evaluate DNA copy number differences on chromosome 4 (performed by
162 NimbleGen Systems Inc). Test samples (patients 3 and 7) were labeled with Cy-3 and the reference sample
163 was labeled with Cy-5. The data were visualized using SignalMap software (NimbleGen). The array was
164 designed, and labeling, hybridization and normalization were performed at NimbleGen. Subsequent
165 analysis was performed in-house.

166 *Long range PCR*

167 Potential breakpoints for a CNV of interest 5' of *CYP4V2* were identified by visual inspection of array CGH
168 data. Primers were designed approximately 2kb 5' and 500bp 3' of the maximal predicted CNV region, with
169 the following sequences: *CYP4V2* F2 5'-CAAGGACTCATCCTGATCAC-3' and *CYP4V2* R1 5'-
170 AGCCTAGTGAGCTTGTCACA-3'. Long range PCR was performed using the Bio-X-Act Long kit (Bioline)
171 following manufacturer's protocols, with >10ng template DNA, 1.5mM Mg²⁺ and cycling conditions of 95°C
172 2 minutes, 60°C 1 minute, followed by 35 cycles of 95°C 30 seconds, 60°C 30 seconds and 68°C 20 minutes,
173 with a final extension step of 68°C for 20 minutes.

174 *Quantitative PCR (qPCR)*

175 Nine pairs of primers were designed at regular intervals across the *CYP4V2* region, from approximately
176 25kb 5' of the gene to approximately 15kb 3', using Primer3 (<http://frodo.wi.mit.edu/>. Accessed March 13,
177 2012), sequences and PCR conditions are given in **Table 1** (available at <http://aaojournal.org>). Quantitative
178 PCR (qPCR) was performed using QuantiFast (Qiagen) following manufacturer's protocols. Reactions were
179 performed on a Step One Plus real time PCR system (Applied Biosystems) in 25µl total volume, using 10ng
180 diluted DNA as template and with final concentrations of 1µM of each primer. PCR efficiencies were
181 determined using serial dilutions of a control DNA sample. Data was analyzed in Microsoft Excel using the

182 Comparative C_T Method ($\Delta\Delta C_t$), normalizing against the 5' most primer pair, and a pair located in *TMEM107*
183 (chr17:8,076,297-8,079,714).

184 *Statistical analyses*

185 Kaplan Meier survival analysis was used to compare the age of onset of symptoms for different mutations.
186 Median survival time to onset of symptoms was derived from the Kaplan Meier product limit estimators.
187 Visual acuity was converted from Snellen acuity into LogMAR units (Logarithm of the Minimum Angle of
188 Resolution) and analyzed as the algebraic mean of two eyes, the better seeing eye, and the worse seeing
189 eye. LogMAR was grouped into 4 categories as <0.3, 0.3≤LogMAR<0.5, 0.5≤LogMAR<1 and ≥1 and analyzed
190 as an ordinal variable. Severity of disease and electrophysiological abnormalities (no, mild and severe
191 generalized retinal dysfunction) were also analyzed as ordinal variables using Fisher's exact test (univariate
192 analyses) and ordinal logistic regression (adjusting for age and gender). Additional patient data was
193 extracted from a publication by Lai et al.¹⁵ and used for pooled analyses. SAS version 9.2 (SAS Institute, Cary
194 NC) was used for analyses.

195 **Results**

196 *Clinical presentation*

197 The clinical phenotypes are summarized in **Table 2** (available at <http://aaojournal.org>). There was marked
198 intra- and inter-familial variability. The 20 patients, 10 male and 10 female, ranged in age from 19 to 72
199 years (median 40 years). Visual acuity varied from 6/5 to perception of light (median 0.3 logMAR, 6/12).
200 The onset of symptoms varied from 22 -45 years, with most patients (n=15, 75%) presenting in the third or
201 fourth decade of life with reduced central vision (n=12) and/or nyctalopia (n=6); 2 patients were
202 asymptomatic at the time of presentation and detected through presentation for unrelated conditions (e.g.
203 corneal foreign body). Visual acuity was highly variable and was not age-related (**Table 2**, available at
204 <http://aaojournal.org>). For example, patient 13 had 6/6 vision in both eyes aged 40 years, whereas patient
205 6 had only perception of light vision in both eyes at a similar age. Five patients (25%) had moderate myopia
206 (-3 to -5 dioptres) while the others were emmetropic or had low myopia. Family GC19455 showed a
207 pseudodominant mode of inheritance with an affected father and two affected sons from a
208 consanguineous family. All other patients were simplex cases, with 1 pair of affected dizygotic twins

209 (patients 1 and 2, GC5048), and an affected sibling of patient 8 (not included in this study as not a patient of
210 this center). A sample of pedigrees is provided in **Figure 1** (available at <http://aaojournal.org>).
211 On clinical examination all patients had retinal crystals at the posterior pole with varying degrees of RPE
212 and inner choroidal atrophy. Four patients from different families (20%) had crystalline deposits at the
213 corneal limbus, and all had either stage 2 or 3 disease. Patients 1 and 2 (GC5048) were dizygotic twin sisters
214 from a non-consanguineous pedigree with a somewhat discordant phenotype; patient 1 had an earlier
215 onset of disease (age 29), vision of 6/60 in both eyes, stage 3 disease and undetectable PERGs in keeping
216 with severe macular dysfunction and ERG evidence of generalized rod and cone photoreceptor dysfunction.
217 Her sibling had onset of symptoms 4 years later (age 33), vision of 6/12 in both eyes, a similar appearance
218 of sparse retinal crystals and widespread atrophy (stage 3) but with less severe macular and generalized
219 retinal dysfunction than her sister (**Table 2**, available at <http://aaojournal.org>). In GC19455 both the older
220 son (proband, patient 13) and father (patient 12) had stage 1 disease localized to the macula, while the
221 younger son (patient 14) had stage 3 disease with a much greater extent of involvement despite being the
222 youngest affected in the pedigree. However, in general, older patients had fewer crystals and more severe
223 retinal atrophy.

224 *Retinal Imaging*

225 Color, AF and SD-OCT scanning of patients with different presentations is shown in **Figure 2**. Areas of RPE
226 and choroidal atrophy tend to develop at the posterior pole, become confluent and expand centrifugally to
227 involve peripheral retina. Areas of normal looking retina anterior to the macula showed normal AF (**Figure**
228 **2B**), while involved areas showed abnormal AF which progressed to become sharply demarcated areas of
229 hypo-AF (**Figures 2E, 2K, 2N**). These sharply demarcated areas correspond to relatively abrupt loss of outer
230 retinal layers including the outer plexiform and outer nuclear layers on SD-OCT (**Figure 2F, 2L**).

231 Crystals seen on color photographs were not visualized on FAF but were highly reflective on NIR imaging
232 (**Figures 3A-C; 3E-G**). SD-OCT scans revealed hyperreflective spots located in or on the RPE/Bruch's
233 membrane complex (**Figure 3D, 3H** up arrows) corresponding to these crystals on color and NIR images.
234 The majority of crystals in all patients were located in or on the RPE/Bruch's membrane complex. However,
235 not all hyperreflective lesions seen on SD-OCT spatially associated with crystalline deposits, as shown in

236 **Figure 3H** (down arrow), where the hyperreflective spot in the inner plexiform layer did not correspond to a
237 crystal on either color or NIR images. Outer retinal tubulations were observed in all patients, except patient
238 19, who was also the youngest patient (19 years) in the case series. There were no hyperreflective spots
239 suggestive of crystals in the choroid in any patient.

240 The appearance of a new crystal in the RPE/Bruch's membrane layer of patient 11 in 2012 which was not
241 present in corresponding scans in 2010 is shown in **Figure 4**. The overlying external limiting membrane
242 remained intact above the new crystal. Crystal disappearance was associated with thinning of the
243 RPE/Bruch's membrane layer, loss of the ellipsoid and external limiting membrane layers, and the
244 formation of what is likely to be an early retinal tubulation.

245 *Electrophysiology*

246 Electrophysiology was performed on 11 patients and revealed a range of abnormalities (**Table 2** and **Figure**
247 **5**, both available at <http://aaojournal.org>). The ERGs in five of 5 patients with extensive RPE/choroidal
248 atrophy (patients 1, 2, 6, 11 and 17) showed evidence of generalized rod and cone photoreceptor
249 dysfunction whereas 3 patients with atrophic lesions confined to the maculae (patients 3, 5 and 10) showed
250 restricted loss of cone and/or rod system function (ERG amplitude reduction without delay). Two further
251 patients with focal macular atrophy had normal full-field ERGs (patients 7 and 13). One patient without
252 atrophy had normal ERGs (patient 19).

253 The pattern ERG P50 component, reflecting macular function, was subnormal bilaterally in 9 patients (1-3,
254 6, 7, 10, 11, 13 & 17); unilaterally in 1 (patient 5). Six of 10 patients showed significant P50 component
255 delay bilaterally (patients 2, 3, 5, 6, 10 and 17). There was no clear correlation between the
256 electrophysiological abnormality and age although the youngest patient with macular crystals without
257 atrophy had normal pattern and full-field ERGs (patient 19; age 15 years).

258 *Molecular analysis*

259 Twenty patients from 17 families were screened. Likely disease-causing variants were found in all 34
260 chromosomes from the 17 families and comprised 11 distinct variants in *CYP4V2* (**Table 2**, available at
261 <http://aaojournal.org>, and **Table 3**). The majority (7/11) of the variants were missense mutations.
262 Interestingly, the most common mutation in our cohort was a novel variant c.197T>G (p.Met66Arg) which

263 was seen in 16/34 chromosomes (47%). This variant was identified in a homozygous state in all 11 patients
264 in 8 families of South Asian ancestry (**Table 2**, available at <http://aaojournal.org>), but not in other patients
265 of European, East Asian or Middle Eastern ancestry. Seven further missense mutations were also identified,
266 4 (6/34 chromosomes, 18%) were novel and 3 have been previously described (4/34 chromosomes, 12%).
267 The next most common mutation detected in our cohort was an indel spanning a splice acceptor site,
268 previously shown to cause the in-frame deletion of exon 7³ and this occurred in 6/34 (18%) chromosomes.
269 One instance each of two potential novel splice site mutations and one nonsense mutation completed the
270 spectrum of mutations. The mutations published to date, including the novel variants reported in this
271 study, are represented schematically in **Figure 6** (available at <http://aaojournal.org>) and suggests that there
272 is no significant clustering of the variants, which have been found throughout the entire coding sequence of
273 the gene.

274 *In silico* analysis of these missense variants using three methods, SIFT, Polyphen 2 and pMUT, showed that
275 they are all predicted to be disease-causing by all three methods with the exception of p.Gly26Asp and
276 p.Met66Arg. The p.Gly26Asp change is only reported by Polyphen 2 to be probably damaging, whereas SIFT
277 and pMUT predict it is a tolerated change (**Table 3**). This substitution was only seen in one patient who also
278 had a putative splice-site mutation, c.985+3A>G in intron 7. Analysis of this potential splicing mutation
279 using NetGene2 showed that the donor splice site at the 3' end of exon 7 is abolished when the A at
280 position +3 is changed to a G. This would result in an mRNA that does not splice to exon 8 but adds on 10
281 amino acids before a stop codon truncates it. This patient (patient 5) had relatively mild disease given her
282 age (stage 2, mild full field ERG abnormalities, 55 years) but otherwise had typical BCD with corneal and
283 retinal crystals (**Table 2**, available at <http://aaojournal.org>). The p.Met66Arg substitution which is reported
284 for the first time here is predicted by Polyphen 2 to be benign but SIFT and pMUT both predict it to be a
285 pathological change with good reliability in pMUT. The other predicted splice mutation, c.327+11G>C needs
286 further analysis.

287 Fifteen of the 17 families harbored homozygous mutations. Multiple single nucleotide polymorphisms
288 (SNPs) were also detected (**Table 4**). The most common mutation (16/34 chromosomes) in the present
289 cohort was the novel missense mutation p.Met66Arg. This was identified in the homozygous state in all 8

290 families of South Asian descent. Analysis of 11 SNPs across CYP4V2 (shown in Table 3 but excluding
291 rs35200327) showed that there is an associated haplotype (G-C-C-G-A-C-G-G-C-A-G). This haplotype also
292 occurs in a homozygous state in these patients suggesting a founder effect.

293 *Examining copy number variation (CNV) of CYP4V2*

294 The finding that the majority of our patients had homozygous mutations and were not reported as being
295 from consanguineous families raised the possibility that there may be a common deletion in this region of
296 chromosome 4, making the individuals appear homozygous, when they are really hemizygous for the
297 reported variant. To test this hypothesis, patient 4, a Turkish woman diagnosed in her early 20's, was
298 initially examined. Metaphase spreads were prepared from peripheral blood lymphocytes and a
299 fluorescently labeled probe from a PAC clone (173M11) containing CYP4V2 and a chromosome 4 paint were
300 used to examine the region. This fluorescent *in situ* hybridization (FISH) showed that patient 4 has two
301 copies of the gene (**Figure 7a**, available at <http://aaojournal.org>). Subsequently samples were obtained
302 from the family (GC17557) and analysis showed each parent had one wild type CYP4V2 and one mutated
303 copy (c.677T>A, p.Met226Lys), and that her 2 siblings harbored two wild type copies (**Figure 7b**, available at
304 <http://aaojournal.org>). Patient 8 was used as a control as he was a compound heterozygote and FISH
305 confirmed he also had 2 copies of the gene as expected (data not shown). Analysis of this family (GC4795)
306 demonstrated that his father was a carrier of a missense mutation (c.1503G>A, p.Arg400His) and his
307 mother a carrier of the splice mutation c.802-8_810del17insGC (**Figure 1**, available at
308 <http://aaojournal.org>).

309 In order to determine whether other members of the cohort exhibiting apparent homozygosity across the
310 gene might instead have a CNV, DNA was sent for array comparative genomic hybridization (aCGH) analysis.
311 DNA from patients 3 and 7 (European and of South Asian descent respectively) were analyzed using a
312 custom array designed to cover this region of chromosome 4. Probes were 20bp apart for the region of
313 interest on chromosome 4 and 250bp apart for the rest of chromosome 4. Nimblegen analysis indicated a
314 deletion in patient 7 and a duplication in patient 3, spanning ~4.8kb in the region chr4:187,093,500-
315 187,098,300 (Hg19), approximately 15kb 5' of CYP4V2 (**Figure 8**, available at <http://aaojournal.org>). This is a
316 region of known copy number variability (Database of Genomic Variants; <http://projects.tcag.ca/variation/>).

317 Accessed March 12, 2012), and is mainly non-genic, with the exception of ~300bp of the 3' untranslated
318 region on FAM149A, the gene immediately flanking CYP4V2 upstream. To further explore the role of CNVs
319 in CYP4V2, qPCR analysis of the region spanning chr4:187,088,471-187,149,502 (from ~25kb 5' of CYP4V2
320 to ~15kb 3') was performed on three patients (patients 3, 5, and 7). The placement of the primers was
321 designed to detect CNVs within CYP4V2, rather than in the potential 5' CNV indicated by the Nimblegen
322 data. The results provided no convincing evidence of CNVs in CYP4V2 in any of these three patients (data
323 not shown). These data support the assertion that these probands were homozygotes rather than
324 hemizygotes for mutations in CYP4V2.

325 *Genotype-phenotype correlations*

326 The patients displayed wide phenotypic variability; the oldest patient (patient 12, 72 years, homozygous
327 p.Met66Arg) had one of the mildest phenotypes (stage 1), while one of the younger patients (patient 6, 39
328 years, heterozygous deletion exon 7) had one of most severe phenotypes (stage 3).

329 Mutations were grouped into 3 categories, those homozygous for p.Met66Arg (n=11), homozygous or
330 heterozygous for other substitutions (n=5) and homozygous or heterozygous for deletion of exon 7 (n=4)
331 and tested for associations with clinical features (**Table 5**, available at <http://aaojournal.org>). Survival
332 curves for age to first onset of symptoms suggested those with the p.Met66Arg mutation or deletions had
333 an earlier onset of symptoms (median age of onset 30 years for both groups) compared to those with other
334 substitutions (median age 41 years), although these differences did not reach statistical significance (p log
335 rank=0.17, **Table 5**, available at <http://aaojournal.org>, **Figure 9A**). Combining the present data with
336 published results from Lai et al.¹⁵ (12 patients heterozygous or homozygous for deletions, 6 heterozygous
337 or homozygous for other substitutions) strengthened the impression of earlier onset of symptoms for
338 p.Met66Arg homozygotes (**Figure 9B**), and the log rank test reached statistical significance (p=0.03). Mean
339 visual acuity was worse for patients with deletions (6/60) compared to those with p.Met66Arg (6/18) or
340 other substitutions (6/15) in the present cohort but these differences did not reach statistical significance.
341 Including patients from Lai et al.¹⁵ and adjusting for age and gender reinforced these impressions but the
342 differences remained non-significant (p>0.05, data not shown). The analyses were repeated for visual
343 acuity in the better, and in the worse seeing eye, with similar results. All (4/4, 100%) patients with deletion

344 of exon 7 had stage 3 disease compared with 5/11 (45%) for those with p.Met66Arg and 3/5 (60%) for
345 those with other substitutions. Similarly, all (3/3, 100%) with deletions had severe generalized full field ERG
346 abnormalities compared with 2/5 (40%) patients with p.Met66Arg and none with other substitutions. These
347 differences did not reach statistical significance both before and after adjustment for age and gender.

348 **Discussion**

349 To date, most patients with BCD that have been reported are of East Asian descent^{3, 5, 15-25} where the
350 prevalence of BCD seems to be higher.²⁶ The present study of British multi-ethnic patients shows significant
351 variability in both phenotypic presentation and severity of disease consistent with prior reports in Asian
352 cohorts and suggests other gene and environmental interactions.^{4, 5, 7-9}

353 Few previous studies to date have utilized FAF imaging in BCD.^{4, 5, 8} The present study found that areas of
354 uninvolved peripheral retina on color images correspond to areas of normal FAF, while areas of involved
355 retina start out as areas of abnormal FAF and progress to become sharply demarcated areas of hypo-AF.
356 These hypo-AF areas represent areas of RPE cell loss and their well defined edges correspond to areas of
357 abrupt outer retinal atrophy on SD-OCT. Similar SD-OCT appearances occur in other diseases with a
358 postulated primary RPE pathology such as gyrate atrophy and choroideremia.²⁷ The lack of AF associated
359 with the crystals themselves is consistent with suggestions that the crystals in BCD may represent
360 collections of cholesterol esters from abnormal lipid metabolism,²⁸ although the precise composition of the
361 crystals remains unclear.²⁹

362 There has been controversy as to the location within the retina of the crystalline deposits in BCD. Some
363 report hyperreflective spots on the RPE/Bruch's membrane complex on SD-OCT,⁴ while others have
364 reported similar looking hyperreflective spots throughout the neurosensory retina and choroid^{6, 8, 9} which
365 has been interpreted as crystal deposition occurring throughout the retina and choroid. Using SD-OCT with
366 co-registration of lesions to NIR images, the vast majority of crystals in the present series were either on or
367 in the RPE/Bruch's membrane complex with a small number of crystals located elsewhere in the retina.
368 There were none in the choroid. Many hyperreflective spots on SD-OCT did not correspond to crystals or
369 any other visible abnormality on either NIR or color images; these may be related to clusters of
370 inflammatory cells, a gliotic response to retinal degeneration³³ protein deposits or simply artefacts. In

371 patient 19 it is clear that the crystals are an early manifestation of the disorder, and need not be
372 accompanied by altered retinal function.⁶

373 The evolution of crystals documented using serial SD-OCT imaging showed that in the early stages crystals
374 appear in the RPE/Bruch's membrane complex with preservation of the overlying external limiting
375 membrane. Atrophy and thinning of the RPE/Bruch's membrane complex was associated with
376 disappearance of the crystals, as well as loss of the photoreceptor ellipsoid and external limiting membrane
377 layers and formation of outer retinal tubulations. These findings are consistent with the clinical
378 observations that despite the presence of numerous crystals there can be relatively preserved visual acuity
379 (cases 10 and 17) or normal macular function (patient 19), while the loss of crystals over time is associated
380 with expanding RPE and inner choroidal atrophy and loss of macular function (patients 1, 3, 7). It can be
381 speculated that crystals may be a visible phenotype of metabolic dysfunction in RPE or photoreceptor cells
382 and their disappearance associated with cell death. It has not been possible to determine if crystals are
383 intra- or extracellular deposits, although histopathological studies report the presence of crystalline
384 intracellular inclusions in extraretinal lymphocytes and fibroblasts in patients with BCD.^{28, 29} Tubulations,
385 believed to be photoreceptor rosettes, have previously been reported in BCD, as well as multiple other
386 conditions, including age-related macular degeneration, pseudoxanthoma elasticum and gyrate atrophy^{30, 31}
387 and suggests that the site of initial dysfunction is likely to be the RPE, with photoreceptor degeneration a
388 secondary consequence.

389 Delayed and subnormal ERGs consistent with generalized rod and cone dysfunction were present in all
390 cases with extensive RPE and choroidal atrophy (**Table 2**, available at <http://aaojournal.org>). Mildly reduced
391 rod- and/or cone-mediated ERGs without delay suggest restricted loss of retinal function and occurred in
392 those with focal areas of macular atrophy. Other patients showed no full-field ERG abnormality. Previous
393 studies report full-field ERGs ranging from normal to undetectable, with most having generalized rod and
394 cone system involvement.^{5, 15, 28, 32-34} Serial ERG data are not available for the present cohort, but
395 progressive ERG worsening has been documented by others.^{32, 33} Multifocal ERG reduction and delay have
396 also been reported in keeping with macular dysfunction^{5, 15} and it is of interest that a high proportion of the
397 present series showed significant PERG P50 delay, with or without amplitude reduction; in general, delays

398 in P50 occur less frequently in genetically determined macular dysfunction than amplitude reduction, and
399 rarely occur unaccompanied by amplitude reduction.

400 Eleven sequence variants were identified, 7 of which are novel and the majority of which are missense
401 mutations (accounting for 74% of chromosomes in this cohort), in contrast to previous observations
402 indicating the most common variant is the deletion c.802-8_810del17insGC.^{24, 35} A review of the literature
403 by Xiao et al. shows that this deletion accounts for 63% of the mutated alleles reported to date in patients
404 of Chinese or Japanese origin.²⁴ The most common mutation (16/34 alleles) in the present cohort was a
405 novel missense mutation p.Met66Arg. This was identified in the homozygous state in all 8 families of South
406 Asian descent, suggesting that exon 1 should be screened first in such patients; just as patients of East
407 Asian descent should have exon 7 screened first to exclude the indel c.802-8_810del17insGC. Interestingly,
408 this novel substitution appeared to be associated with an earlier onset of symptoms. This finding should be
409 interpreted with caution as it may be related to biases such as recall bias (i.e. the two sons in family
410 GC19455 with an affected parent may be more aware of symptoms and hence report earlier onset) and
411 issues with pooling data from another centre in a different country and health system¹⁵ Nonetheless, this
412 substitution still appears to be related to earlier onset of symptoms even after excluding data from family
413 GC19455 and Lai et al.¹⁵ The specific amino acid sequence and surrounding region is highly conserved in
414 mammals but not in non-mammalian animals or invertebrates.

415 In terms of clinical severity, patients with deletions seemed to have more severe disease and worse visual
416 acuity. The 17bp deletion (c.802-8_810del17insGC) includes the exon 7 splice acceptor site and so causes
417 an in-frame deletion of exon 7 that would result in expression of a truncated 463 amino acid protein.³ This
418 deletion has previously been reported to be associated with a more severe ERG phenotype.¹⁵

419 Since 2004 there have been 20 reports, including this one, documenting over 50 different mutations in
420 *CYP4V2*.^{3, 5, 6, 8, 15, 36-39} The missense and nonsense mutations reported to date are summarized in **Figure 6**,
421 available at <http://aojournal.org>. *CYP4V2* is an 11 exon gene encoding a predicted protein of 525 amino
422 acids, with mutations identified across the entire gene (**Figure 6**, available at <http://aojournal.org>). A
423 recent study by Nakano and colleagues reported p.H331P as the most common missense mutation,
424 accounting for 7% of all mutated alleles, compared to the 63% of alleles with the c.802-8_810del17insGC

425 deletion.⁴⁰ They went on to demonstrate that the p.H331P mutant encodes an unstable protein. This is the
426 only report showing that a change in CYP4V2 results in a non-functional protein. Further studies need to be
427 undertaken to determine the effect of the other described missense and nonsense mutations on the
428 function of CYP4V2.

429 A number of biochemical findings indicate systemic abnormalities of lipid metabolism in patients with
430 BCD.^{41, 42} CYP4V2 is the most distinct of the human CYP4 family with only ~35% sequence identity to other
431 family members.⁴³ The encoded protein is a microsomal omega (ω)-hydroxylase that functions together
432 with mitochondrial and peroxisomal β -oxidation enzymes to degrade cellular lipids, with a preference for ω -
433 3 polyunsaturated fatty acids (PUFA)s such as docosahexaenoic acid (DHA) and eicosapentaenoic acid
434 (EPA).⁴⁴ These PUFAs are important constituents of photoreceptor outer segments that are recycled by RPE
435 cells. In addition to being structural components, some PUFA derived metabolites e.g. resolvin and
436 protectin possess anti-inflammatory and immunoregulatory signaling properties which may be disrupted by
437 mutations in CYP4V2.⁴³ The protein is expressed in human RPE, retina, cornea and many other tissues
438 including kidney, liver, lung and lymphocytes.^{3, 40} Its phenotypic effects may be most prominent in the RPE
439 where it appears to be the primary CYP4 protein expressed.⁴⁰ Together with the presented imaging data,
440 such evidence further implicates the RPE as the cellular site of dysfunction in BCD. Given that the
441 therapeutic window from onset of symptoms to severe vision loss is a decade or more, this offers the
442 possibility of pharmacologic intervention to delay progression.

443 This study was not prospective and although all available data are presented for all patients, it is inevitable
444 that patients seen earlier before the introduction of new imaging modalities did not have these performed.
445 Six patients had complete imaging and ERG assessment. It is possible that this may have introduced a bias
446 but we believe this is unlikely as the six patients with complete assessments are a representative sample
447 that spans a large age range (15-40 years at time of ERGs) and the full spectrum of severity on both ERG
448 and clinical severity

449 In conclusion, this report expands and refines the phenotypic characteristics of Bietti Crystalline Dystrophy.
450 FAF showed sharply demarcated areas of RPE loss which coincided with abrupt edges of outer retinal
451 atrophy on SD-OCT. The crystals, which are best visualized using NIR imaging and which are not evident on

452 FAF imaging, are shown by SD-OCT to be located on or in the RPE/Bruch's membrane complex; this
453 combined with other data suggests that RPE dysfunction underlies disease pathogenesis. The mutation
454 spectrum in this multi-ethnic British cohort, including novel mutations, differs to that previously described
455 in other populations.

456

457 **Acknowledgments**

458 We also wish to thank Professor Alison Hardcastle, Institute of Ophthalmology for useful discussions on the
459 array CGH data and Dr. Alex Morris, Imperial College for help with the haplotype analysis.

460

461

462

References

- 463 1. Okialda KA, Stover NB, Weleber RG, Kelly EJ. Bietti Crystalline Dystrophy. 1993. In: Pagon RA, Adam
464 MP, Bird TD, et al, eds. Gene Reviews [database online]. Available at:
465 <http://www.ncbi.nlm.nih.gov/books/NBK91457/>. Accessed August 1, 2013.
- 466 2. Jiao X, Munier FL, Iwata F, et al. Genetic linkage of Bietti crystalline corneoretinal dystrophy to
467 chromosome 4q35. *Am J Hum Genet* 2000;67:1309-13.
- 468 3. Li A, Jiao X, Munier FL, et al. Bietti crystalline corneoretinal dystrophy is caused by mutations in the
469 novel gene *CYP4V2*. *Am J Hum Genet* 2004;74:817-26.
- 470 4. Kojima H, Otani A, Ogino K, et al. Outer retinal circular structures in patients with Bietti crystalline
471 retinopathy. *Br J Ophthalmol* 2012;96:390-3.
- 472 5. Lee KY, Koh AH, Aung T, et al. Characterization of Bietti crystalline dystrophy patients with *CYP4V2*
473 mutations. *Invest Ophthalmol Vis Sci* 2005;46:3812-6.
- 474 6. Manzouri B, Sergouniotis PI, Robson AG, et al. Bietti crystalline retinopathy: report of retinal crystal
475 deposition in male adolescent siblings. *Arch Ophthalmol* 2012;130:1470-3.
- 476 7. Pennesi ME, Weleber RG. High-resolution optical coherence tomography shows new aspects of
477 Bietti crystalline retinopathy. *Retina* 2010;30:531-2.
- 478 8. Rossi S, Testa F, Li A, et al. Clinical and genetic features in Italian Bietti crystalline dystrophy
479 patients. *Br J Ophthalmol* 2013;97:174-9.
- 480 9. Toto L, Carpineto P, Parodi MB, et al. Spectral domain optical coherence tomography and in vivo
481 confocal microscopy imaging of a case of Bietti's crystalline dystrophy. *Clin Exp Optom* 2013;96:39-45.
- 482 10. Yuzawa M, Mae Y, Matsui M. Bietti's crystalline retinopathy. *Ophthalmic Paediatr Genet* 1986;7:9-
483 20.
- 484 11. Weleber RG, Wilson DJ. Bietti's crystalline dystrophy of the cornea and retina. In: Heckenlively JR,
485 Arden GB, eds. Principles and Practice of Clinical Electrophysiology of Vision. 2nd ed. Cambridge, MA: MIT
486 Press; 2006:735-44.
- 487 12. Marmor MF, Fulton AB, Holder GE, et al, International Society for Clinical Electrophysiology of
488 Vision. ISCEV standard for full-field clinical electroretinography (2008 update). *Doc Ophthalmol*
489 2009;118:69-77.
- 490 13. Holder GE, Brigell MG, Hawlina M, et al, International Society for Clinical Electrophysiology of
491 Vision. ISCEV standard for clinical pattern electroretinography (2007 update). *Doc Ophthalmol*
492 2007;114:111-6.
- 493 14. Bach M, Brigell MG, Hawlina M, et al. ISCEV standard for clinical pattern electroretinography
494 (PERG): 2012 update. *Doc Ophthalmol* 2013;126:1-7.
- 495 15. Lai TY, Ng TK, Tam PO, et al. Genotype phenotype analysis of Bietti's crystalline dystrophy in
496 patients with *CYP4V2* mutations. *Invest Ophthalmol Vis Sci* 2007;48(11):5212-20.
- 497 16. Gekka T, Hayashi T, Takeuchi T, et al. *CYP4V2* mutations in two Japanese patients with Bietti's
498 crystalline dystrophy. *Ophthalmic Res* 2005;37:262-9.
- 499 17. Haddad NM, Waked N, Bejjani R, et al. Clinical and molecular findings in three Lebanese families
500 with Bietti crystalline dystrophy: report on a novel mutation. *Mol Vis* [serial online] 2012;18:1182-8.
501 Available at: <http://www.molvis.org/molvis/v18/a124/>. Accessed August 1, 2013.
- 502 18. Jin ZB, Ito S, Saito Y, et al. Clinical and molecular findings in three Japanese patients with crystalline
503 retinopathy. *Jpn J Ophthalmol* 2006;50:426-31.
- 504 19. Lin J, Nishiguchi KM, Nakamura M, et al. Recessive mutations in the *CYP4V2* gene in East Asian and
505 Middle Eastern patients with Bietti crystalline corneoretinal dystrophy [report online]. *J Med Genet*
506 2005;42:e38. Available at: <http://jmg.bmj.com/content/42/6/e38.full.pdf+html>. Accessed August 1, 2013.
- 507 20. Shan M, Dong B, Zhao X, et al. Novel mutations in the *CYP4V2* gene associated with Bietti crystalline
508 corneoretinal dystrophy. *Mol Vis* [serial online] 2005;11:738-43. Available at:
509 <http://www.molvis.org/molvis/v11/a87/>. Accessed August 1, 2013.
- 510 21. Zenteno JC, Ayala-Ramirez R, Graue-Wiechers F. Novel *CYP4V2* gene mutation in a Mexican patient
511 with Bietti's crystalline corneoretinal dystrophy. *Curr Eye Res* 2008;33:313-8.
- 512 22. Wada Y, Itabashi T, Sato H, et al. Screening for mutations in *CYP4V2* gene in Japanese patients with
513 Bietti's crystalline corneoretinal dystrophy. *Am J Ophthalmol* 2005;139:894-9.
- 514 23. Yokoi Y, Nakazawa M, Mizukoshi S, et al. Crystal deposits on the lens capsules in Bietti crystalline
515 corneoretinal dystrophy associated with a mutation in the *CYP4V2* gene. *Acta Ophthalmol* 2010;88:607-9.

- 516 24. Xiao X, Mai G, Li S, et al. Identification of CYP4V2 mutation in 21 families and overview of mutation
517 spectrum in Bietti crystalline corneoretinal dystrophy. *Biochem Biophys Res Commun* 2011;409:181-6.
- 518 25. Rossi S, Testa F, Li A, et al. An atypical form of Bietti crystalline dystrophy. *Ophthalmic Genet*
519 2011;32:118-21.
- 520 26. Hu DN. Ophthalmic genetics in China. *Ophthalmic Paediatr Genet* 1983;2:39-45.
- 521 27. Lazow MA, Hood DC, Ramachandran R, et al. Transition zones between healthy and diseased retina
522 in choroideremia (CHM) and Stargardt disease (STGD) as compared to retinitis pigmentosa (RP). *Invest*
523 *Ophthalmol Vis Sci* 2011;52:9581-90.
- 524 28. Wilson DJ, Weleber RG, Klein ML, et al. Bietti's crystalline dystrophy: a clinicopathologic correlative
525 study. *Arch Ophthalmol* 1989;107:213-21.
- 526 29. Kaiser-Kupfer M, Chan C, Markello T, et al. Clinical biochemical and pathologic correlations in
527 Bietti's crystalline dystrophy. *Am J Ophthalmol* 1994;118:569-82.
- 528 30. Sergouniotis PI, Davidson AE, Lenassi E, et al. Retinal structure, function, and molecular pathologic
529 features in gyrate atrophy. *Ophthalmology* 2012;119:596-605.
- 530 31. Zweifel SA, Engelbert M, Laud K, et al. Outer retinal tubulation: a novel optical coherence
531 tomography finding. *Arch Ophthalmol* 2009;127:1596-602.
- 532 32. Jurklies B, Jurklies C, Schmidt U, Wessing A. Bietti's crystalline dystrophy of the retina and cornea.
533 *Retina* 1999;19:168-71.
- 534 33. Yanagi Y, Tamaki Y, Takahashi H, et al. Clinical and functional findings in crystalline retinopathy.
535 *Retina* 2004;24:267-74.
- 536 34. Chen H, Zhang M, Huang S, Wu D. Functional and clinical findings in 3 female siblings with
537 crystalline retinopathy. *Doc Ophthalmol* 2008;116:237-43.
- 538 35. Mackay DS, Halford S. Focus on molecules: cytochrome P450 family 4, subfamily V, polypeptide 2
539 (CYP4V2). *Exp Eye Res* 2012;102:111-2.
- 540 36. Garcia-Garcia GP, Lopez-Garrido MP, Martinez-Rubio M, et al. Genotype-phenotype analysis of
541 Bietti crystalline dystrophy in a family with the CYP4V2 Ile111Thr mutation. *Cornea* 2013;32:1002-8.
- 542 37. Mamatha G, Umashankar V, Kasinathan N, et al. Molecular screening of the CYP4V2 gene in Bietti
543 crystalline dystrophy that is associated with choroidal neovascularization. *Mol Vis* [serial online]
544 2011;17:1970-7. Available at: <http://www.molvis.org/molvis/v17/a214/>. Accessed August 1, 2013.
- 545 38. Song Y, Mo G, Yin G. A novel mutation in the CYP4V2 gene in a Chinese patient with Bietti's
546 crystalline dystrophy. *Int Ophthalmol* 2013;33:269-76.
- 547 39. Yokoi Y, Sato K, Aoyagi H, et al. A novel compound heterozygous mutation in the CYP4V2 gene in a
548 Japanese patient with Bietti's crystalline corneoretinal dystrophy. *Case Rep Ophthalmol* [serial online]
549 2011;2:296-301. Available at: <http://www.karger.com/Article/Abstract/331885>. Accessed August 1, 2013.
- 550 40. Nakano M, Kelly EJ, Wiek C, et al. CYP4V2 in Bietti's crystalline dystrophy: ocular localization,
551 metabolism of omega-3-polyunsaturated fatty acids, and functional deficit of the p.H331P variant. *Mol*
552 *Pharmacol* 2012;82:679-86.
- 553 41. Lee J, Jiao X, Hejtmancik JF, et al. Identification, isolation, and characterization of a 32-kDa fatty
554 acid-binding protein missing from lymphocytes in humans with Bietti crystalline dystrophy (BCD). *Mol*
555 *Genet Metab* 1998;65:143-54.
- 556 42. Lee J, Jiao X, Hejtmancik JF, et al. The metabolism of fatty acids in human Bietti crystalline
557 dystrophy. *Invest Ophthalmol Vis Sci* 2001;42:1707-14.
- 558 43. Kelly EJ, Nakano M, Rohatgi P, et al. Finding homes for orphan cytochrome P450s: CYP4V2 and
559 CYP4F22 in disease states. *Mol Interv* 2011;11:124-32.
- 560 44. Nakano M, Kelly EJ, Rettie AE. Expression and characterization of CYP4V2 as a fatty acid omega-
561 hydroxylase. *Drug Metab Dispos* 2009;37:2119-22.

562
563
564
565

Table 3. *In silico* analysis of missense mutations in *CYP4V2*

Exon	Mutation	SIFT		Polyphen 2		pMUT			References
		Prediction	Tolerance index	Prediction	Score	NN output	Reliability	Prediction	
1	c.77G>A, p.Gly26Asp	Tolerated	0.21	PRD	0.989	0.3834	2	Neutral	Novel to this study
1	c.197T>G p.Met66Arg	Intolerant	0.02	Benign	0.009	0.8042	6	Pathological	Novel to this study
2	c.283G>A, p.Gly95Arg	Intolerant	0.01	PRD	1.000	0.8878	7	Pathological	6, 23
6	c.677T>A, Met226Lys	Intolerant	0.00	PRD	0.989	0.6214	2	Pathological	Novel to this study
8	c.998C>A, p.Thr333Lys	Intolerant	0.00	PRD	1.000	0.8480	6	Pathological	Novel to this study
9	c.1503G>A, p.Arg400His	Intolerant	0.00	PRD	1.000	0.5805	1	Pathological	18, 23, 27
10	c.1393A>G, p.Arg465Gly	Intolerant	0.00	PRD	1.000	0.6607	3	Pathological	8

SIFT¹⁵ results are reported to be tolerant if tolerance index ≥ 0.05 or intolerant if tolerance index < 0.05

Polyphen 2¹⁶ appraises mutations qualitatively as Benign, PossiblyDamaging (POS) or Probably damaging (PRD) based on the model's false positive rate

pMUT¹⁷ is based on the use of different kinds of sequence information to label mutations, and neural networks to process this information NN=neural network values from 0 to 1. > 0.5 is predicted as a disease associated mutation. Reliability=values 0–9. > 5 is the best prediction

Table 4. SNPs identified in *CYP4V2*

rs number	Exon/intron	Nucleotide	Amino acid	dbSNP MAF (minor allele frequency)
rs1055138	Exon 1	c.64C>G	p.Leu22Val	G=0.4390
rs10013653	Intron 1	c.215-22C→A		A=0.4222
rs7682918	Intron 2	c.327+75C→T		T=0.3201
rs35200327	Intron 3	c.412_414delCT		NA
rs4862662	Intron 4	c.605-25G→T		T=0.3512
rs13146272	Exon 6	c.775C>A	p.Gln259Lys	C=0.4547
rs3817184	Intron 6	c.802-7C→T		0.424
rs34745240	Exon 7	c.823G>A	p.Glu275Lys	A=0.0298
rs3736455	Exon 7	c.810T>G	p.Ala270Ala	T=0.4492
rs3216724	Intron 8	c.1090+99delC		-=0.326
rs2276918	Intron 9	IVS9+45A→G		G=0.3365
rs72646291	Exon 10	c.1328G>A	p.Arg443Gln	A=0.0018

Figure 2

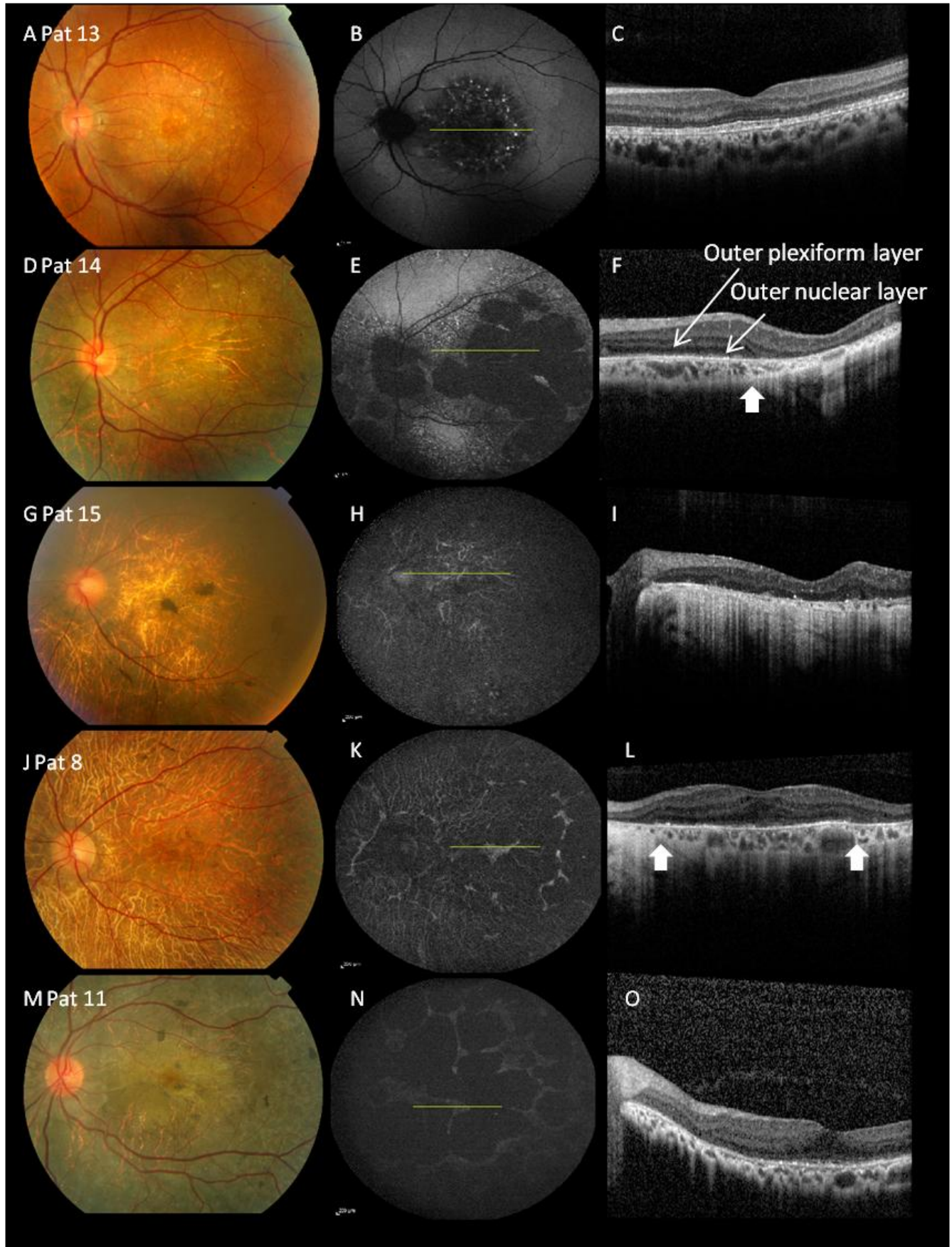


Figure 3

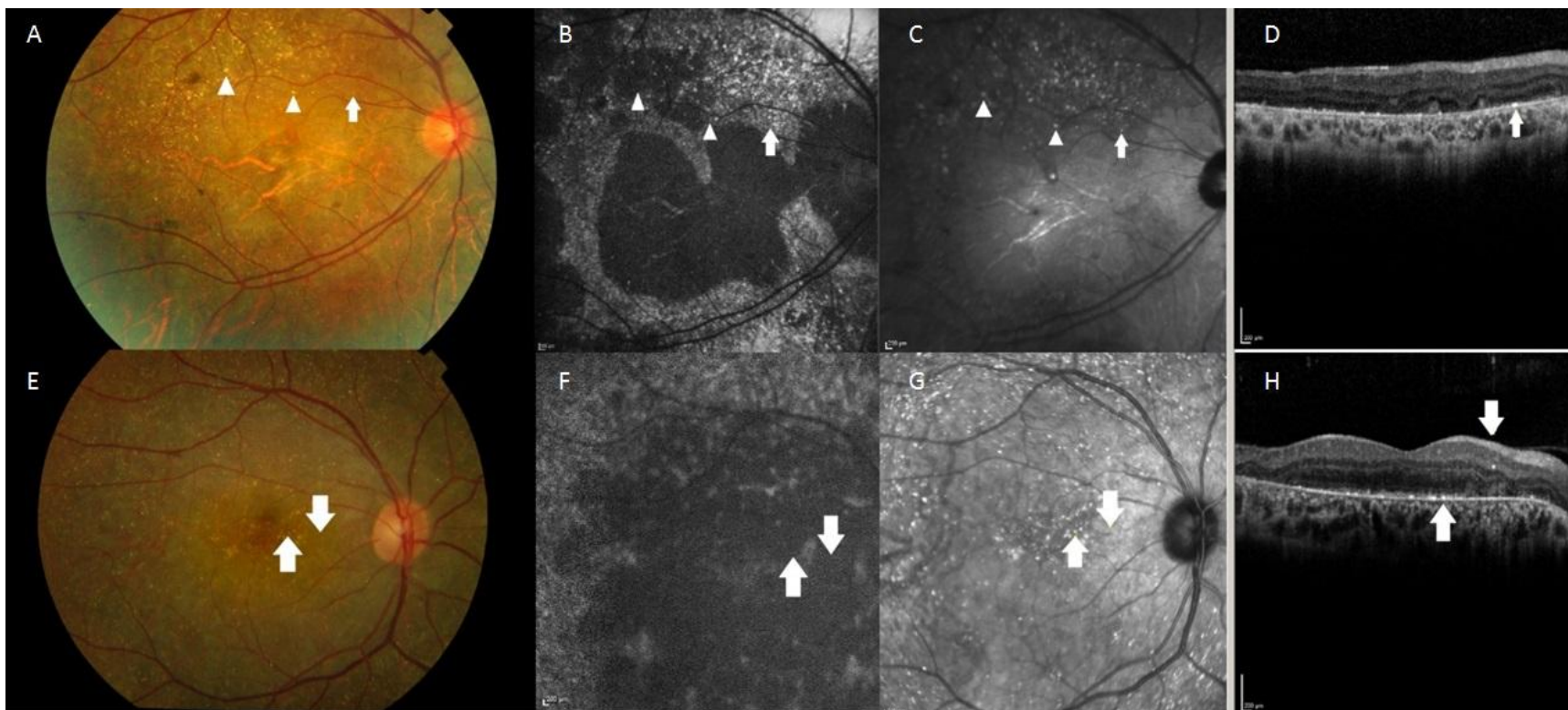


Figure 4

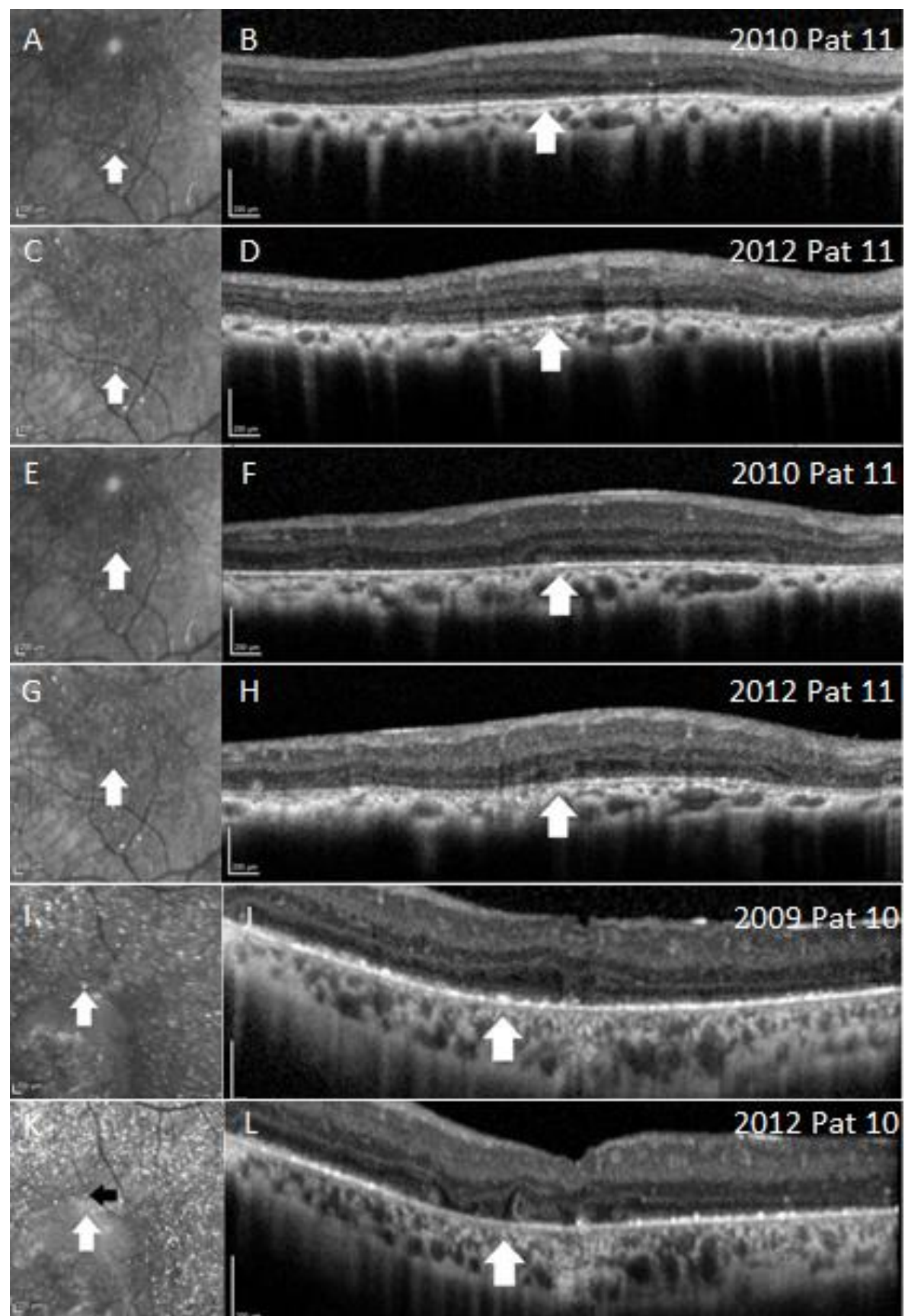
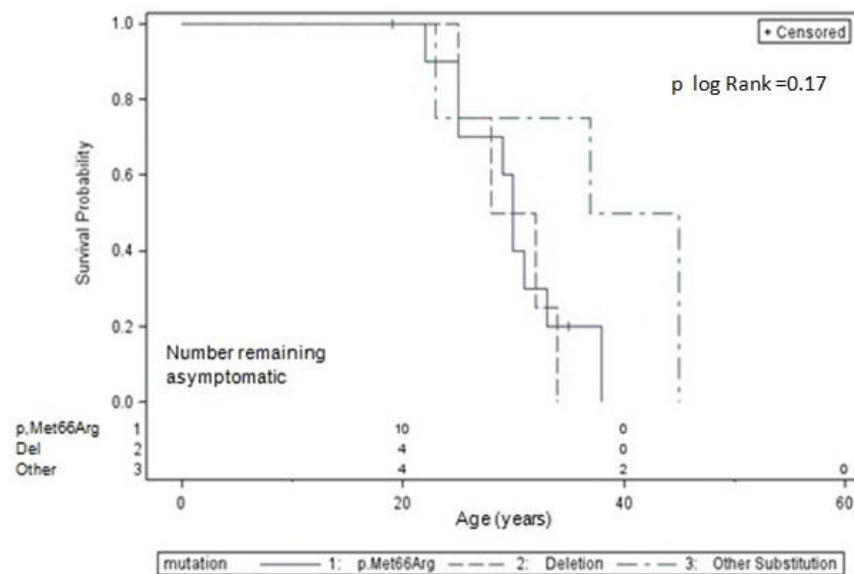


Figure 9

A. Survival curves of time to onset of symptoms by mutation, patients from this sample (n=19)



B. Survival curves of time to onset of symptoms by mutation, patients from this sample plus those of Lai et al (n=37)

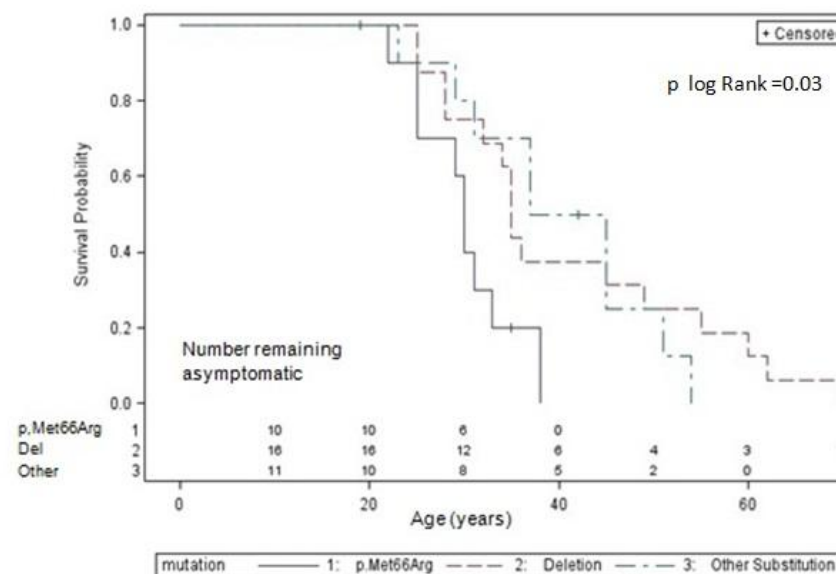


Figure Legends

Figure 2. Color imaging, fundus autofluorescence (AF) and Spectral domain Optical Coherence Tomography (SD-OCT) imaging.

Color, AF and SD-OCT scanning of patients with different presentations, patient 13 panels **A-C**; patient 14 panels **D-F**; patient 15 panels **G-I**; patient 8 panels **J-L** and patient 11 panels **M-O**. Panels **A-C** from patient 13 show localized disease confined to the macula. Areas of normal looking retina on color images (**A**) show normal AF (**B**). Affected areas (**B**) show disrupted outer retinal layers on SD-OCT (**C**). Panels **D-F** from patient 14 (younger brother of patient 13) show more severe disease with more widespread abnormalities on AF (**E**). The sharp transition from abnormal AF to hypo-AF (**E**) corresponds on OCT (**F**) to a fairly abrupt transition from relatively intact retinal layers to loss of outer retinal layers including the outer plexiform and nuclear layers (up arrow). Panels **G-O** show patients with more severe, generalized disease and low AF suggesting widespread loss of retinal pigment epithelium (RPE). In patient 8, the central island of relatively preserved retina (**J**) on AF (**K**) corresponds to relatively preserved outer retinal layers on OCT (**L**) and highlights again the sharp demarcation (up arrows) between this preserved island and the surrounding hypo-AF retina (**K**) and atrophic outer retinal layers (**L**). Patient 11 (**M**) illustrates the usefulness of AF in demonstrating the clearly defined areas of RPE loss with a small island of preserved central retina (**N**), that is also visible on SD-OCT (**O**).

Figure 3. Color photographs of crystals and corresponding appearances on autofluorescence (AF), near infra-red and spectral domain optical coherence tomography (SD-OCT).

Patient 14 panels **A-D**; patient 19 panels **E-H**. Color photograph showing crystals (**A**, arrows, arrowheads, patient 14). Crystals are neither hyper nor hypo-AF (**B**) but show up clearly on near infra-red imaging (**C**). SD-OCT shows that the crystals are located in or on the retinal pigment epithelium/Bruch's membrane layer (**D**, arrow). A similar appearance is shown for crystals in a different patient (**E-H**, up arrow, patient 19); however in that case a hyperreflective spot in the inner

plexiform layer on SD-OCT (**H**, down arrow) does not correspond to a crystal on either color photography, AF or near infra-red (**E-G**).

Figure 4. Longitudinal evolution of crystals over 2-3 years.

Comparative scans from Patient 11 are shown from 2010 and 2012 (**A-H**) and from patient 10 from 2009 and 2012 (**I-L**). Panels **A-D** show the appearance of a new crystal in the retinal pigment epithelium (RPE) /Bruch's membrane layer in 2012 (**C, D** arrows), which was not present in 2010 (**A, B** patient 11). Panels **E** and **F** from the same patient in 2010 show a crystal in the RPE/Bruch's membrane complex with a granular appearance to the overlying ellipsoid line and external limiting membrane. Between 2010 and 2012, this crystal disappeared on both near infra-red and Spectral domain Optical Coherence Tomography (SD-OCT) scanning, with disruption and loss of the RPE/Bruch's membrane and overlying ellipsoid (photoreceptor) and external limiting membrane (**G,H**). Figures I-L compare images obtained in 2009 with those obtained in 2012 for patient 10. In panel **I** there is a crystal at the margin of an atrophic zone, which on SD-OCT imaging (**J**) has a present ellipsoid line and to a lesser extent, external limiting membrane line. Over 3 years, the area of atrophy expanded (**K**) with disappearance of the crystal on near infra-red and appearance of a new crystal (black arrow, **K**). The disappearance of the crystal corresponds to thinning of the RPE/Bruch's membrane layer, loss of ellipsoid and external limiting membrane lines, and the formation of possible early tubulation (**L**).

Figure 9. Kaplan Meier survival curves for survival time to first onset of symptoms by mutation type. Panel A includes patients from this study; Panel B also incorporates data from Lai et al.¹⁵ Patients with p.Met66Arg mutations had earlier onset of symptoms than those with other substitutions (p logrank=0.03). Patient 12 was excluded from analyses due to uncertain age of onset of symptoms

***Copyright SH & SB**

[Click here to download Copyright: Copyright form SH & SB.pdf](#)

***Copyright loO**

[Click here to download Copyright: Copyright form loO.pdf](#)

***Copyright DM**

[Click here to download Copyright: Copyright form DM.pdf](#)

***Copyright EV**

[Click here to download Copyright: Copyright form EV.pdf](#)

***Copyright LO**

[Click here to download Copyright: Copyright Form LO.pdf](#)

***Copyright PS**

[Click here to download Copyright: Copyright form PS.pdf](#)

***Copyright RH**

[Click here to download Copyright: Copyright form RH.pdf](#)

*Conflict of Interest Form (ICMJE COI) SH

[Click here to download Conflict of Interest Form \(ICMJE COI\): coi_disclosure SH.pdf](#)

*Conflict of Interest Form (ICMJE COI) GL

[Click here to download Conflict of Interest Form \(ICMJE COI\): coi_disclosure_GL.pdf](#)

*Conflict of Interest Form (ICMJE COI) DM

[Click here to download Conflict of Interest Form \(ICMJE COI\): coi_disclosure_DM.pdf](#)

*Conflict of Interest Form (ICMJE COI) PS

[Click here to download Conflict of Interest Form \(ICMJE COI\): Sergouniotis-coi_disclosure.pdf](#)

*Conflict of Interest Form (ICMJE COI) RH

[Click here to download Conflict of Interest Form \(ICMJE COI\): coi_disclosure_RH.pdf](#)

*Conflict of Interest Form (ICMJE COI) SB

[Click here to download Conflict of Interest Form \(ICMJE COI\): coi_disclosure_SB.pdf](#)

*Conflict of Interest Form (ICMJE COI) EV

[Click here to download Conflict of Interest Form \(ICMJE COI\): coi_disclosure EV.pdf](#)

*Conflict of Interest Form (ICMJE COI) LO

[Click here to download Conflict of Interest Form \(ICMJE COI\): coi_disclosure_LO.pdf](#)

*Conflict of Interest Form (ICMJE COI) AR

[Click here to download Conflict of Interest Form \(ICMJE COI\): coi_disclosure_AGR.pdf](#)

*Conflict of Interest Form (ICMJE COI) GH

[Click here to download Conflict of Interest Form \(ICMJE COI\): coi_disclosure_GH.pdf](#)

*Conflict of Interest Form (ICMJE COI) AT

[Click here to download Conflict of Interest Form \(ICMJE COI\): coi_disclosure_ATM.pdf](#)

*Conflict of Interest Form (ICMJE COI) MM

[Click here to download Conflict of Interest Form \(ICMJE COI\): coi_disclosure_MM.pdf](#)

*Conflict of Interest Form (ICMJE COI) AW

[Click here to download Conflict of Interest Form \(ICMJE COI\): coi_disclosure_AW.pdf](#)

Supplemental Material Figure 1

[Click here to download Supplemental Material: Halford, Liew et al. Ophthalmology Figure 1.pdf](#)

Supplemental Material Figure 5

[Click here to download Supplemental Material: Halford, Liew et al. Ophthalmology Figure 5.pdf](#)

Supplemental Material Figure 6

[Click here to download Supplemental Material: Halford, Liew et al. Ophthalmology Figure 6.pdf](#)

Supplemental Material Figure 7

[Click here to download Supplemental Material: Halford, Liew et al. Ophthalmology Figure 7.pdf](#)

Supplemental Material Figure 8

[Click here to download Supplemental Material: Halford, Liew et al. Ophthalmology Figure 8.pdf](#)

Supplemental Material Table 1

[Click here to download Supplemental Material: Halford Liew et al. Ophthalmology Table 1.pdf](#)

Supplemental Material Table 2

[Click here to download Supplemental Material: Halford, Liew et al. Ophthalmology Table 2.pdf](#)

Supplemental Material Table 5

[Click here to download Supplemental Material: Halford, Liew et al. Ophthalmology Table 5.pdf](#)

permission for acknowledgments

[Click here to download Supplemental Material: Emails from AH and AM.pdf](#)